PROCEEDINGS, 44th Workshop on Geothermal Reservoir Engineering
Stanford University, Stanford, California, February 11-13, 2019
SGP-TR-214

Geothermal Exploration North of Mount St. Helens: Washington State Play-Fairway Project

Drew Spake[1], Alexander N Steely[2], Trenton T. Cladouhos[3], Michael W. Swyer[3], Corina Forson[2], Nicholas C. Davatzes[1]

[1]Temple University, Philadelphia, PA 19125

[2]Washington Geological Survey, MS 47007, Olympia, WA 98504-7007

[3]formerly at AltaRock Energy, now a Cyrq Energy, Suite 400, 4010 Stone Way N., Seattle, WA 98103Mailing address, on one line

Drew.spake@temple.edu

Keywords: Play-Fairway, Washington State, St. Helens Seismic Zone, fracture, porosity, drill, geothermal exploration, geomechanics, resource assessment

ABSTRACT

Active seismicity within a broad zone in proximity to volcanism in the St. Helens Seismic Zone north of Washington State's Mount Saint Helens provide key ingredients for hydrothermal circulation at depth. This seismicity extends well north of the volcanic edifice below where several faults and associated fractures in outcrop record repeated slip, dilation and alteration indicative of localized fluid flow. Candidate reservoir rocks include marine metasediments overlain by extrusive volcanics. This study characterizes the faults and fractures in the extrusives which are available in outcrop and sampled along well TGH17-24 and Plate Boundary Observatory strainmeter borehole, B201. Outcrop mapping and borehole image log analysis down to 250 m document abundant volcaniclastic deposits and basalt flows that are highly fractured, although intervening ash layers truncate the vertical extent of many of these structures. However, strike slip faults with well-developed gouge zones and adjacent localized high fracture density provide potential for vertically extensive fracture flow paths. Where these rocks are altered by intrusion, they develop high fracture density that can support heat transfer. Borehole image logs further record breakout that indicate the azimuth of S_{Hmax} in the shear zone is approximately 054/234°±23.6°, consistent with seismically active strike slip faults in the seismic zone, faults mapped in outcrop and evident in the borehole image logs, and with of plate convergence data. Temperature profiles in two wells indicate isothermal conditions at average groundwater temperatures, consistent with rapidly flowing water localized within fractures.

1. INTRODUCTION

Despite active volcanism, geothermal energy remains an under-utilized resource in the Cascades region of the Pacific Northwest. Lack of development partly reflects difficulty in locating potential reservoirs due to a strong groundwater masking effect coupled with lack of outcrop exposure for geological characterization. The Geothermal Play-Fairway Analysis (PFA) for Washington State developed and implemented an exploration methodology (Forson, 2015; Forson et al., 2015; Forson et al., 2016; Forson et al., 2017; Swyer, et al., 2016) to improve the search for blind geothermal systems by assessing the likelihood for colocation of essential elements of a complete geothermal system including: (a) a heat source, (b) a permeable conduit connecting the heat source to (c) shallow porous and permeable reservoir rocks that are (d) saturated. One of the sites identified with a high potential for each of these characteristics, as well as necessary infrastructure and development, is approximately 15 km north of Mount St. Helens within the NNW-SSE trending St. Helens Seismic Zone (SHSZ).

Essential to this methodology is that actively slipping faults and secondary fractures generate and maintain connected porosity necessary to host a geothermal system. The presence of such connected porosity and either hot water indicating active geothermal circulation or hydrothermal alteration consistent with fossil circulation provide necessary tests of this critical hypothesis.

This relationship is being tested by two field studies which began in the summer of 2018. First, the potential for fault-related porosity is assessed through outcrop and petrographic mapping of faults and fractures and their associated porosity and alteration. This investigation at the surface is extrapolated to depth by analysis of image and petrophysical logs in the Plate Boundary Observatory (PBO) borehole B201. Together, these studies characterize the geometry, kinematics, and associated healing or alteration of the fracture and fault population. The goal is to determine if faults and fractures in basalt flows or indurated volcaniclastic deposits at reservoir depths are likely to provide connected porosity sufficient to host commercially viable geothermal reservoirs. An important factor is their stratigraphic arrangement, since ash falls and hydrothermally altered units may act as barriers to connectivity. Furthermore, borehole wall failure in image logs of B201 and slickenlines on the mapped faults provide new constraints on the regional geomechanical model. Second, the presence of heat is assessed with a temperature-gradient hole (TGH) drilled in the summer of 2018 with plans for further deepening in 2019; temperature logs and analysis of the cuttings provide new information on thermal resources. In this paper, we: 1) review fault-associated porosity in the Mount St. Helens study area, and 2) present preliminary drilling results from the 2018 campaign. As a result of these two investigations, we present a refined and tested conceptual model of geothermal systems in the vicinity of Mount St. Helens.

1.1 Play Fairway Analysis at Mount Saint Helens

At Mount St. Helens, the hypothesized geothermal resource is heated by young intrusives related to the magmatic plumbing system beneath the volcanic edifice and transported along the SHSZ to potential shallow reservoirs (Forson et al., 2017) (Figure 1). The dominant lithologies within the SHSZ consist of extrusive flows and volcaniclastic deposits underlain by marine metasediments which are bound on either side by two large, low porosity igneous plutons (Evarts et al., 1987; Evarts and Ashley, 1993). Reservoirs within the SHSZ would then be hosted in the fractured extrusive flows, volcaniclastic deposits and metasediments, with fluid recharged by meteoric water, which may be sealed from surface expression by a hydrothermally altered, clay-rich caprock. Repeated, dilatant slip of fractures within the actively deforming SHSZ creates and maintains the fluid storage and its connection to the heat source critical to a geothermal reservoir.

This conceptual model was devised by the PFA, which is a collaborative project headed by the Washington Geological Survey and AltaRock Energy with support from the Department of Energy's Geothermal Technologies Office. Phases 1 and 2 produced and refined statewide maps of geothermal favorability, and selected sites at which to test the methodology and assess the presence of heat by drilling temperature gradient holes (Forson, 2015; Forson et al., 2015; Forson et al., 2016; Forson et al., 2017). In the summer of 2018, Phase 3 commenced at Mount St Helens, resulting in partial drilling of TGH 17-24 sited above seismic velocity anomalies suggesting fluid filled fractures below (Waite and Moran, 2009; Swyer et al., 2018).

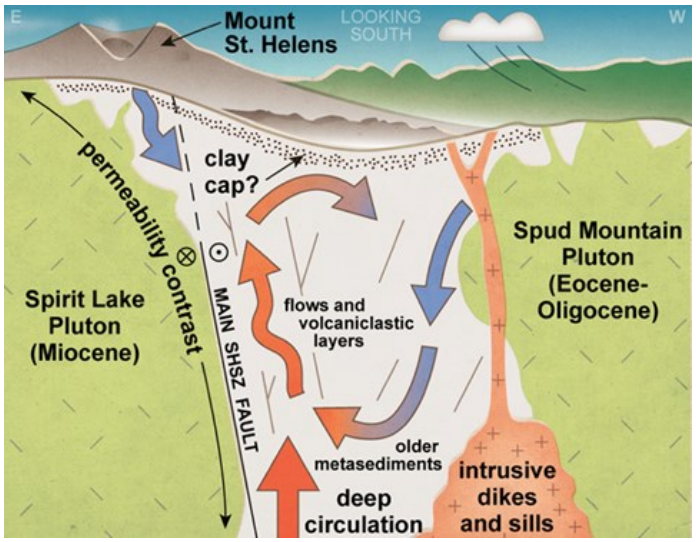

Figure 1: Schematic diagram of the geothermal system at Mount St. Helens (reproduced from Forson et al., 2017).

2. GEOLOGICAL SETTING

Mount St. Helens (MSH) is a quaternary stratovolcano in southwestern Washington with an underlying small, shallow magma body between depths of 7 and 18 km (Barker and Malone, 1991; Anderson and Segall, 2013) revealed by an aseismic volume within an active cloud of microseismicity and modeling of surface deformations from GPS and strainmeters. Although there are extensive studies on seismicity in the area following the 1980 eruption, relatively little is known of bedrock stratigraphy. The volcano was built on top of an area of highly eroded, folded, and altered volcanic and plutonic rocks that range from 28 to 22 Ma. The bottom of the section consists of basalt and basaltic andesite, while the upper portion is andesitic and dacitic (Evarts et al., 1987).

Mount St. Helens is situated at a 25° bend in the highly active St. Helens Seismic Zone that extends both North and South of the edifice. In combination with focal mechanisms, the seismicity in the more active northern SHSZ defines a set of steeply dipping, NNW-SSE trending strike-slip faults (Swyer et al., 2016) also evident in detailed topography derived from LiDAR. Due to the right-lateral motion of slip on the SHSZ, the dextral offset creates extension within a volume of crust between the offset segments; Weaver et al. (1987) have interpreted this right-stepping offset of the SHSZ with older fractures to control the transport of magma through the crust to the volcanic edifice, thereby controlling the spatial position of the volcano. Geologic mapping conducted in Phase 2, and expanded in this paper, identified faults whose attitudes and slickenlines indicate paleo-stress similar in orientation to the modern stress state (S_{Hmax} approximately N – S) inferred from focal mechanisms and from geodetic analysis (Swyer et al., 2016; Forson et al., 2017). This indicates that the mapped faults have the potential to be active (Forson et al., 2017).

Earthquake epicenters near Mount St. Helens delineate a zone of active seismicity characterized by frequent, small magnitude events with prominent clusters below the volcanic edifice, as well as to the north and south of the volcano (Figure 2a). The targets for geothermal exploration are 10 km to the north of MSH along the SHSZ, outside of the protected national monument. Although not definitive, the events located below target TGH sites to the north of MSH are consistent with brittle failure in the SHSZ that could facilitate movement of fluids from heat sources associated with MSH to the north. Potential reservoirs along this path and below the

TGH wells include marine metasediments overlain by extrusive volcanics. Despite have two distinct candidates, this study focuses on the potential role of extrusive volcanics taking advantage of their exposure at the surface.

The PFA team posits that geothermal heat is transported along fracture and fault permeability in the SHSZ from deep magmatic sources closer to MSH (Forson et al., 2017).

Below MSH, is a narrow vertical zone of seismicity (Figure 2b); at shallow depth, this seismicity is interpreted to reflect hydrothermal circulation and magma movement (Barker and Malone, 1991, whereas seismicity greater than ~18 km is interpreted to reveal the conduit that delivers magma to the volcano (Waite and Moran, 2012). Figure 2b further reveals vertically extensive clusters of seismicity in the SHSZ to the north and south of MSH. Focal mechanisms indicate a predominance of strike slip motion consistent with mapped fault traces in the SHSZ (Weaver and Smith, 1983; Weaver et al., 1987; Li, 1988; Swyer et a., 2016). The PFA interprets these clusters to indicate active fault slip that may support dilation and thus promote the crustal circulation of fluid necessary to support a geothermal system. The clusters occur in discrete time intervals (Figure 2b), often show a typical main-shock aftershock sequence, also consistent with the damage model proposed by the PFA to induce fracture-hosted porosity (Swyer et al., 2016; Forson et al., 2017).

The PFA drill sites (black triangles) are located above the northern clusters of seismic activity near the intersection of modeled faults (Swyer et al., 2016; Forson et al., 2017). The Plate Boundary Observatory's borehole strainmeter B201 (hereafter referred to as B201) is near the PFA sites, within the SHSZ. Three other borehole strainmeters encircle the volcano, both within and outside of the SHSZ, though these will not be discussed within the scope of this paper.

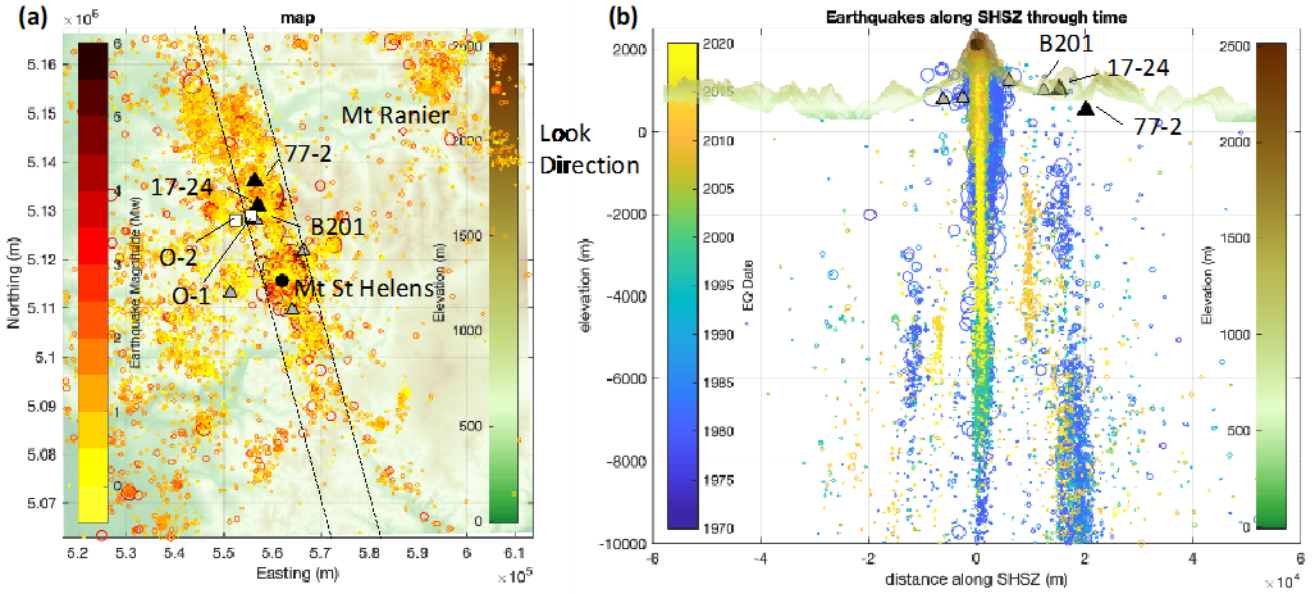

Figure 2: (a) Map showing seismicity, topography, PFA drill sites, PBO borehole strainmeters, and outcrop map sites relative to Mount Saint Helens and the SHSZ. Bubbles correspond to earthquake epicenters scaled and colored by magnitude from the USGS Earthquake Catalogue, 1970-2019. (b) Cross-section of seismicity within and along the SHSZ as viewed from the ENE toward WSW. Circle size corresponds to magnitude as in (a) but color corresponds to time (10x vertical exaggeration).

2.1 Outcrop and Thin Section Locality

Important issues in locating blind geothermal systems in the Cascades Mountains are the dense vegetation that ubiquitously covers terrain to the West of the range, and the massive amount of rainfall this area receives. This thick ground cover makes access to bedrock outcrops severely limited in most cases, while cold precipitation suppresses common surface expressions of geothermal systems, such as hot springs and fumaroles (Forson et al., 2017). The issue is mitigated to some degree in the area north of Mount St. Helens due to the infrastructure in place to support both the National Monument and the logging land operated by Weyerhauser Corporation and Noble Farms, on which the PFA drill sites are located.

Two outcrops were selected near the TGH sites to characterize the patterns of fractures, their associated alteration, and any dependence on rock type or position in the SHSZ.Outcrop map were made at two locales, one representing the interior of the SHSZ and another at the SHSZ margin (Figure 2). Outcrop 1 exemplifies a typical stratigraphic package in the SHSZ comprised of basalt flows, volcaniclastics, and ash fall, and thus demonstrates the association of stratigraphy and rock type with fracture and fault characteristics.

Outcrop 2 juxtaposes these same rock types against the intrusive Spud Mountain Pluton at the margin of the SHSZ. This juxtaposition demonstrates the relationship between proximity to a fossil heat source with fracture and fault characteristics and associated alteration.

2.2 PBO Borehole Strainmeter Locality

PBO borehole strainmeter B201 is located just north of Coldwater Lake and only 3 km SSW of PFA drill site 17-24. Geophsycial logs from this hole provide a test of the relationships between rock type, fracture populations, and fluid flow predicted by the PFA model. Results from image log interpretation are combined with outcrop and thin section scale investigations to evaluate the model of porosity production and maintenance at depth in the SHSZ.

Whereas the 17-24 drill site targeted a location where the PFA methodology predicted high geothermal potential, B201 is located at a nearby site with comparatively low favorability. The difference is that 17-24 site coincides with the intersection of modeled fault segments and their mechanical effects (Swyer et al., 2016), a critical element of the PFA assessment of storage and permeability. This difference in favorability over a distance of 3 km also highlights the difficulty that small-scale heterogeneity poses to exploration of geothermal systems, and for which the PFA model was specifically developed (Forson, 2015; Forson et al., 2015; Forson et al., 2016; Forson et al., 2017; Swyer, et al., 201). By probing both sites of high and low potential, we provide a more complete test of the PFA approach to these critical elements– although both sites are limited by relatively shallow total depths.

3. RESULTS

3.1 Review of Fracture Characteristics

In the brittle upper crust, zones of high porosity may be created and maintained by active fault slip due to accompanying dilation (e.g., Caine et al., 1995; Townend and Zoback, 2001). The fractures most likely to slip are those oriented to maximize the ratio of shear to normal traction, often referred to as "critically stressed." Barton et al. (1998) demonstrated that in the Dixie Valley geothermal field, the majority of hydraulically conductive fractures are critically stressed. Mickelthwaite and Cox (2006) applied this concept to ore deposits, suggesting that the mechanism operates over the long time scales necessary to accumulate ores. These studies, along with analyses of aftershocks and induced earthquakes, suggest relatively little stress change is necessary to reactivate faults (e.g. McGarr et al., 1978; King et al., 1994).

Dilation is strongly influenced by host rock properties such as mineralogy, rock strength, and initial surface roughness of fracture walls (e.g., Davatzes and Hickman, 2010; Wells and Davatzes, 2015). Mineralogy and rock strength are strongly related; minerals with high frictional strength and slip-weakening behavior tend to promote dilation during slip in the shallow crust (Lockner and Beeler, 2003). For these minerals, recurrent brittle fracture can thus induce dilation owing to the effects of surface roughness on the walls of fault planes (Brown, 1987). The resulting connected porosity increases permeability across the rock volume. In contrast, frictionally weaker minerals, especially phyllosilicates such as smectite and illite, tend to inhibit dilation during slip (e.g. Davatzes and Hickman, 2010). Thus mineral types and relative abundance provide an indication of rock strength due to the differences in material strength for common rock forming and alteration minerals, as well as fracture or fault permeability (Crawford et al., 2003; Tembe et al., 2010 and references therein; Zhu, 2012). At the outcrop scale, evidence of dilation includes veins and the textures and mineralization of slip surfaces. The history of surface modification and exposure to fluids is also revealed through petrographic analysis of fractures and the adjacent host rock. This has the further benefit of establishing the relative timing of mineralizations (paragenesis), which is used as a proxy for fluid flow history.

To allow for fluid circulation over the 100's of meters to kilometers necessary to support a hydrothermal system also requires an extensive network of connected fractures (Huengres and Ledru, 2011). Connectivity is promoted by a variety of fracture attitudes, high fracture density and fracture intersection characteristics (Eichubl et al., 2009; Davatzes and Hickman, 2010). The types and organization of lithologic units can also have a profound control on the dimensions of fractures (e.g. Laubach et al., 2009;). These characteristics are documented by: (a) outcrop maps of fracture and fault spacing, attitude, and kinematics and (b) in the subsurface by characterization of fracture populations from acoustic image logs.

In this study outcrop mapping and petrographic analysis is used to document the detailed geometry of fractures and faults and the influence of lithology. This analysis is extended to depth by assessing fracture attitude and density in lithologic units along the B201 borehole in image logs.

3.2 Field Results

Two key outcrops were mapped in detail for lithology and fracture characteristics to document the dependence of porosity and pore structure on deformation history. Outcrops were digitally mapped on photographic basemaps in the field using criteria as defined below.

3.2.1 Outcrop 1 Lithology

The dominant lithologies found in the field area are Tertiary (i.e. not MSH-aged) volcaniclastic deposits, lithified ash deposits, and basalt flows (Evarts et al., 1987; Evarts and Ashley, 1993) (Figure 3). The term volcaniclastic denotes sedimentary rocks formed by processes resulting from volcanic eruptions, *e.g*. pyroclastic flows, lahars, debris flows. These units are typically highly indurated, and in some locations where the material is fine-grained are difficult to distinguish from basalt in the field. Volcaniclastic unit 1 (*Vcl 1*) has a red-purple groundmass which supports a chaotic arrangement of small clasts, up to a few mm in size. Some of these are small feldspar lathes, while others are amorphous, globular white masses of quartz. Thin section analysis shows that the groundmass is comprised of a trachytic texture of small feldspar psuedomorphs with a preferential grain alignment, and is thus interpreted as an ignimbrite or welded

tuff. These small grains have been heavily altered or totally replaced by kaolinite, as indicated by X-ray Diffraction (XRD). Volcaniclastic unit 2 (*Vcl 2*) is comprised of large boulders and cobbles suspended in a chalky white matrix, likely reflecting deposition by lahar or debris flow. The lithified ash (*Ash*) deposits are stratified in thin layers which are light grey to brown, very fine grained, and friable. Basalt flows (*Basalt flow*) are massive, and in some places along the outcrop display poorly developed columnar jointing. These basalts have a dark green, aphanitic groundmass with phenocrysts of plagioclase, clinopyroxene, and rare olivine.

Outcrop 1 provides a well-exposed example of a typical stratigraphic package in the SHSZ comprised of sequences of volcaniclastics, partially draped by ash, which is itself overlain by a basalt flow. Stations 1 and 2 (Figure 3) show sub-horizontal volcaniclastic interbedded with ash deposits. These layers are topped by a massive, blocky basalt flow. The ash layers pinch-out laterally over distances of tens of meters so that the volcaniclastic and basalt units are intermittently in contact. Several ash layers exhibit soft sediment deformation where the overlying basalt impinges on the ash layer. On the east edge of Station 3, the upper boundary of the volcaniclastic layer (*Vcl 1*) and basalt also thins, thus appearing to define the edge of a paleo-valley into which the basalt flowed.

The organization of lithologic units in outcrop suggests an environment typified by large bodies of laterally extensive and well-lithified volcaniclastics in which ash layers discontinuously drape paleo-topography. Basalt flows are superposed on these layers, are less extensive than volcaniclastics, and may be laterally confined by paleo-valleys. Evarts and Ashely (1993) note that the relative proportions of volcaniclastic versus basalt may vary significantly across the study area.

3.2.2 Outcrop 1 Structures

Fractures are identified as discontinuities in the host rock, are typically steeply dipping, and often display mineral coatings. Care was taken to distinguish these discontinuities from layer boundaries or flow structures which influence weathering and occasionally have the appearance of fractures. Where significant secondary minerals fill a fracture, they are classified as veins accommodating dilation.

Faults are identified by striations, gouge, veins, and offset. Most faults show multiple layers of slip surfaces separated by layers of vein fill, host rock, or gouge. Gouge zones are very fine grained, friable and crumbly, often reddish brown in color, are found adjacent to slip surfaces; they weather to negative relief and are often associated with springs, streams, and dense vegetation, and were thus only observed in excavations.

Well-developed faults characterized by gouge zones several centimeters, or more, thick have adjacent damage zones. In most examples the damage forms fractured-bounded volumes extending up to a few meters from the faults with limited detectable rotation. Two distinct fracture orientations occur: (a) steeply dipping fractures parallel to the fault slip surface that extend the several meters to span the outcrop, and are spaced at two to ten centimeters; (b) small fractures nearly perpendicular to and abutting these fault-parallel fractures. In a few examples, well developed breccias with highly rotated, angular fracture-bound clasts in a matrix of cement occur. This brecciation is limited to within less than one meter from the fault sip surface or gouge zone, and occurs in isolated volumes less than one meter long.

Dikes are also common features in the vicinity of MSH and in the SHSZ to north and south (Evarts and Ashley, 1993). These dikes are typically sub-vertically intruded into volcaniclastic, ashes, and basalt flows. They are typically basaltic to andesitic and aphyric to aphanitic. Closer to MSH, some dikes show flow structure parallel to the margins, but similar examples were not found in the SHSZ in proximity to the drill sites and mapped outcrops. The margin of the dike mapped in Station 4 is well-preserved but lacks a chill margin; similarly, the adjacent formation lacks any clear indication of contact metamorphism. This may imply that the host rock at the time of deposition was relatively warm.

3.2.3 Outcrop 1 – Stratigraphic Controls on Faults and Fractures

These outcrop maps demonstrate three distinct fracture/fault populations and each of their relationships to the different lithologic units.

Fractures: All of the lithologies are cut by vertical to sub-vertical fracture sets lacking vein fill, gouge, or kinematic indicators. However, these fractures are far more abundant in the volcaniclastics and basalt flows than in the ash layers (Figure 3). In general, these fractures are layer-bound, especially where ash layers define the unit boundary. In damage zones adjacent to large faults with well-developed gouge, fractures typically span the width of the layer to extend into adjacent layers.

Normal faults: Conjugate sets of normal faults are evident from the offset of internal layering or of unit boundaries and dip angles from 59-70° are present in all layers. Unlike the fractures discussed above, they often cross layer boundaries, accommodating offset of no more than a few centimeters (Figure 3, Station 1 and 2), but nevertheless are typically shorter than the outcrop height of approximately 7 to 10 meters. However, several of these faults tip out where they cross from the overlying basalt into the underlying ash layer. In these instances, this lower tip curves toward lower angle and parallelism with the fissility of the ash layer. Many of these faults are characterized by vertical segmentation. Overlapping and linkage of these segments define fault-bound rhombohedrons which are variably open, filled with gouge, or filled with white, fine-grained vein materials interpreted as carbonate or zeolites.

Strike slip faults: Strike slip faults are identified as west-southwest striking, steeply dipping structures. These faults are characterized by slickensided surfaces recording shallow rakes and are exposed in the volcaniclastic unit Vcl 1 in this outcrop. Whereas some of these structures are entirely contained within Vcl 1 (Station 3), two prominent faults span all lithologies present and are characterized by well-developed gouge in excess of one meter thick, local brecciation and adjacent damage (Stations 3 and 4). The slip surfaces of all these faults are universally coated with quartz and often chlorite. On the larger faults, multiple layers of quartz have accumulated, and where different layers are exposed, each displays striations. Any single layer may show multiple generations of cross-cutting striations varying

about the typical strike slip rakes. The immediate implication is that these faults accommodated repeated slip and dilation sufficient to accumulate centimeters of cement.

Impact of Stratigraphy: The maps indicate that lithology and stratigraphic boundaries have a strong impact on the dimensions and attitude of brittle structures. The discussion above illustrates that the smaller fractures show a clear difference in attitude, kinematics, and density between rock types, as well as confinement by layer boundaries. We assess this difference by comparing the distribution of the different structure types within each major lithologic unit (Figure 3).

- Basalt layer displays a uniform density of fractures which are largely confined to the stratigraphic unit and do not cross ash layers.

- Small normal faults are equally present in volcaniclastic and basalt layers, but are lower density than fractures. These structures bridge layer boundaries and promote localized fragmentation at the decimeter to meter length-scales.

- Strike slip faults show localized damage revealed by high fracture density adjacent to gouge zones in both volcaniclastics and basalt. These structures appear likely to span multiple stratigraphic layers, and precipitation on slip surfaces, in breccia, and local silicification of adjacent fractures imply they may act as key fluid conduits.

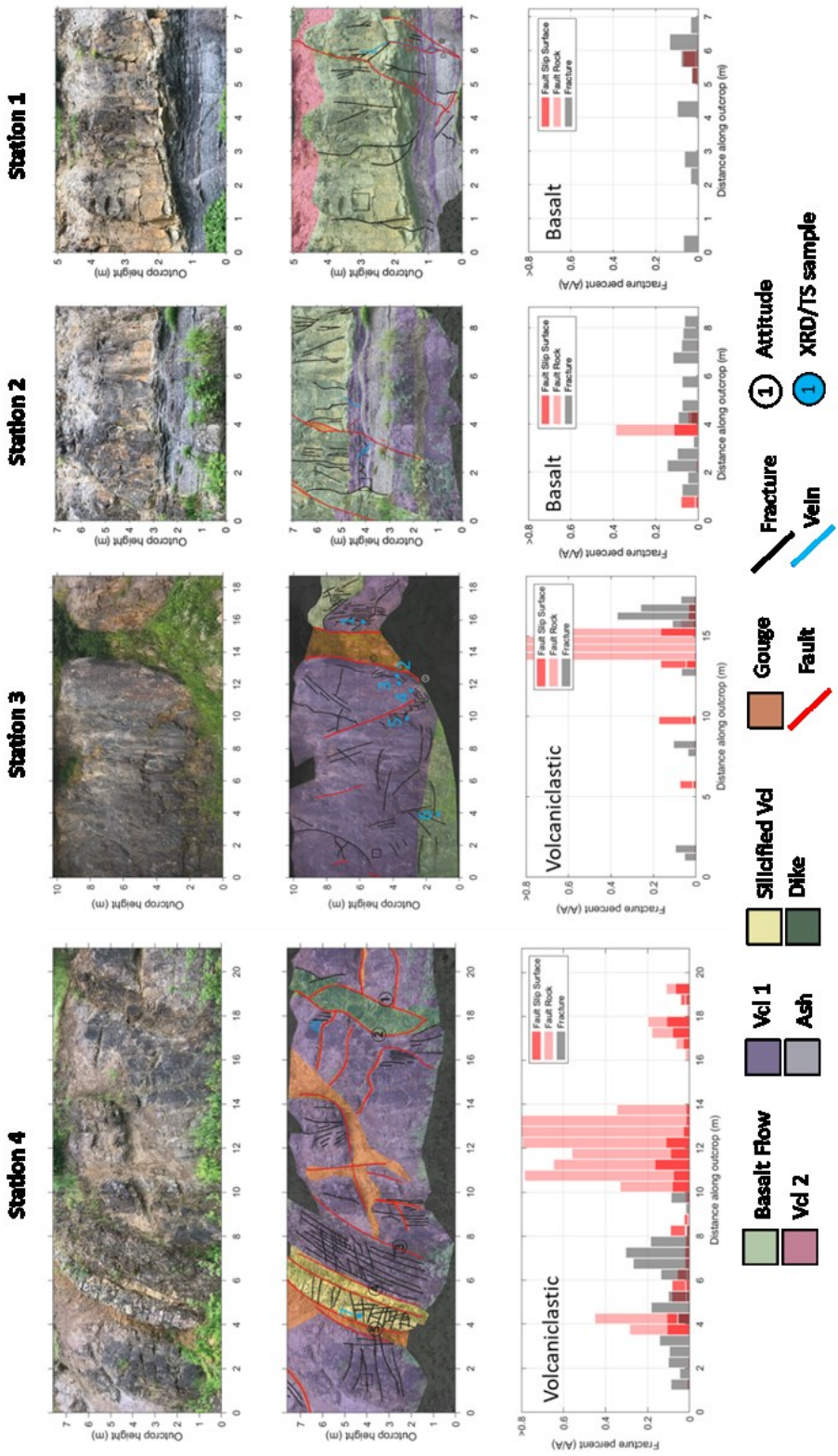

Figure 3: Geological characterization of Outcrop 1: Top Row: Station Photographs of road cut along Hwy. 504; Middle Row: Geologic Maps; Bottom Row: Fracture, Fault, and Fault rock frequency distribution. The stations are numbered from SSE (Station 1) to NNW (Station 4) along the length of a single continuous outcrop. In Stations 3 & 4, blue dots record sample locations used in XRD and petrographic analyses. The histogram is calculated from a 1x1m sample window at a constant y-coordinate, with one box plotted on each map for scale and position.

3.2.4 Outcrop 1 – Fracture Paragenesis

The role of the faults and fractures in fluid flow at Outcrop 1 is assessed by comparing the alteration of rock samples as a function of proximity to the major faults or to smaller associated fractures either in their damage zone or in the set of distributed fractures in the background. Six hand samples were collected from Outcrop 1, Station 3, and one from Station 4 for petrographic analysis (Figure 4).

At Station 3 the volcaniclastic host rock samples have a fine-grained groundmass which have the shape of feldspar microlites, but are currently occupied by clay. XRD indicates the clays are dominated by kaolinite, and only a small fraction of feldspar remains. These pseudomorphs show a preferred orientation, creating a trachytic texture consistent with classification as an ignimbrite or welded tuff. Larger feldspar pseudomorphs stand out from the groundmass in plane polarized light, but in cross polarized light it is clear that they have been similarly altered and replaced. Lithic clasts are present but often difficult to distinguish given the ubiquitous alteration. There is an abundance of small, rounded to angular opaque minerals throughout. There are amorphous globules of microquartz which appear as misshapen white blobs in hand sample or under plane polarized light. Iron oxide staining is distributed randomly throughout the groundmass, giving the samples their characteristic purple-red color in hand sample. Despite this pervasive alteration, in outcrop these rocks are competent and resist weathering.

Quartz, dolomite, and iron-oxide, primarily as hematite with minor goethite, are all found as secondary fracture-filling cements (Figure 4a) in thin sections and verified by XRD. Quartz filled fractures are unique in that they are free of oxides and are cross-cut by both hematite and dolomite filled fractures, making them the earliest phase precipitated. Hematitic veins are precipitated at two distinct times. First, veins filled with hematite crosscut older quartz veins (Figure 4c). These veins are themselves cut by fractures whose walls are coated in hematite and superposed layers of dolomite in the middle of the vein. Later, this vein assemblage is brecciated and the pore space between breccia clasts is filled with hematite (Figure 4a, b) and sheared (Figure 4b). The dolomite veins appear both in isolation as well as in fracture whose walls are coated in hematite. (Figure 4b, c). The general lack of euhedral crystal grains of either quartz or dolomite suggest that both mineral phases are the result of primary precipitation within fractures rather than recrystallized from less stable phases of opal or calcite, respectively. Fractures with the largest aperture are consistently filled with a combination of dolomite and Fe-oxide that show evidence of shearing as well as dilation.

In close proximity to large faults, fractures in the volcaniclastics are often open, lacking healing by secondary mineral precipitation. These open fractures are closely associated with alteration haloes of Fe-oxide staining which extend from the fracture wall into the surrounding host rock. These haloes typically extend ~1 mm from individual fractures. However, where adjacent fractures overlap and create zones of localized extension the intervening space is bridged by many small which are filled with Fe-oxide cement apparently emanating from the open fracture walls. This causes larger zones of alteration, extending several centimeters from the open fracture (Figure 4e, f). In the fragmented Silicified Volcaniclastics (*S-Vcl*) of the damage zone associated with the strike slip faults, alteration of the host rock is advanced and extends much further from the fracture (Figure 4g, h). Pervasive alteration of the rock adjacent to the fracture gives way to unaltered rock in the interior of fracture-bound clasts. The interior of these clasts are comparatively un-fractured, yet exhibit a sharp alteration boundary (Figure 4i, j). These features are interpreted to indicate that such open fractures act as conduits for fluid flow which invades the surrounding host rock.

In contrast, basalt at the base of Station 3 is comparatively un-fractured (Figure 4d) compared to similarly located volcaniclastics. The fractures present are thin and mostly free of cement. The walls of these fractures are covered with a thin coating of iron oxide, which extends as a halo around the fractures, approximately 1 mm to either side of the open space. This implies that both rock type and the structural position relative to the large strike slip faults strongly influence the history of fracture healing and alteration.

Fracture history and paragenesis: Some fractures in basalts, andesites, or volcaniclastics may be initiated by cooling and contraction of these hot deposits, though this is difficult to distinguish in thin section. However, the orientation of splay fractures, brecciation and grain rotation of host rock and fracture-filling cements, and reoccupation of previously healed fractures by different cements are all consistent with dilation that results from shearing. Fractures in thin section reveal at least 4 phases of fracturing and alteration:

(1) Initial fracturing creates open porosity, which is healed by precipitation of quartz cement. Quartz is precipitated over a wide range of temperatures and pH conditions (Huenges and Ledru, 2011), but precipitation is promoted in cooling fluids suggesting either upward circulation or authigenic formation as the hot rock cools following deposition.

(2) A second phase of deformation creates new fractures which are then coated and healed by Fe-oxide cement.

(3) A third phase of deformation creates new fractures and reactivates previously healed fractures, which are then healed by dolomite cement. Evarts and Ashley (1993) report that clay-carbonate assemblages are prominent hydrothermal alteration products around MSH, implying that precipitation of dolomite cement in this outcrop is consistent with circulating hot fluids.

(4) Most recently, reactivation of fractures associated with the strike slip fault have caused fragmentation and local brecciation of these cements, and subsequent precipitation of a new Fe-oxide cement in the surrounding interstitial spaces within the fractures.

(5) Open fractures primarily occur in the damage zones within several meters of the large strike slip faults as well as in the basalt flow. Otherwise, fractures in the volcaniclastics are predominated by healed.

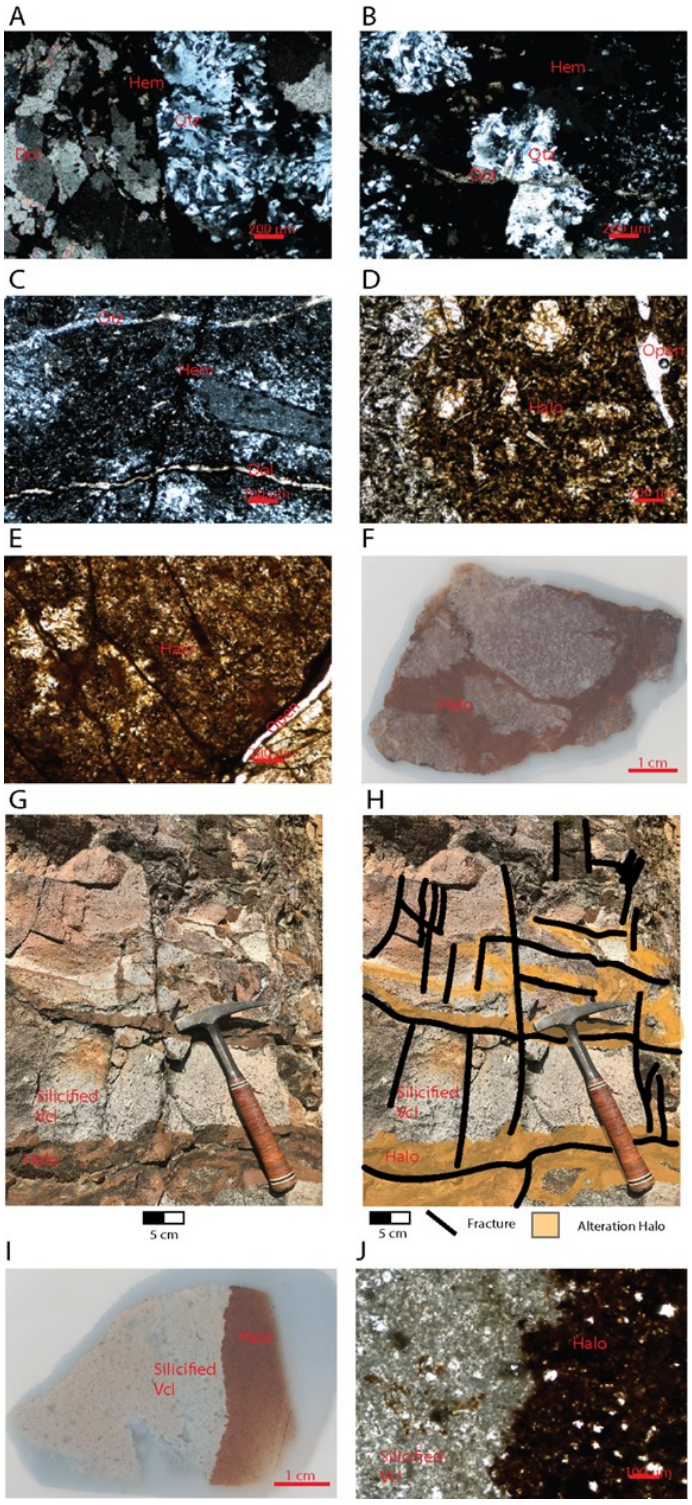

Figure 4: Photographs, high resolution scans, and photo-micrographs of representative structural and lithological features from Outcrop 1. Qtz = quartz. Hem = hematite. Dol = Dolomite. Open = open fracture porosity. Halo = alteration halo. Sample sites are recorded on maps in Figure 4: Station 3: A= B=3; C=4; D=6; E=F=1; Station 4: G=H=I=J=7. (a) and (b) show two views of a fracture containing clasts of broken and rotated cement indicating reactivation in shear and (c) crosscutting and superposition of quartz, then hematite, then dolomite in volcaniclastic rock. (d) fracture and associated alteration halo in basalt. (e) thin section detail of (f) showing an open fracture with iron oxide alteration of wall rock in volcaniclastic rock. (g, h) fractures in silicified volcaniclastics (*S-Vcl*) surrounded by symmetrically developed iron oxide rinds. (i) and (j) show details of the transition from iron oxide to silicified volcaniclastic in (g, h).

3.2.5 Outcrop 2 – Lithology

This outcrop juxtaposes volcaniclastic rock against a finger of the 24 Ma Spud Mountain Pluton (Figure 5). The outcrop therefore displays varying degrees of contact metamorphism and hydrothermal alteration as function of distance from the intruded body and faults cross-cutting the outcrop. Maps of this outcrop are used to investigate how host rock, fracture, and fault characteristics are modified by exposure to a heat source with the goal of understanding how they might ultimately support a magmatically driven geothermal system. Rock designations distinguish degree of alteration leading to new local rock units ultimately derived from potentially the same original volcaniclastic deposit.

Volcaniclastic 1 (*Vcl 1*) has a greenish groundmass in which a chaotic arrangement of feldspar grains, rare amphibole, and abundant small lithic clasts are suspended. Volcaniclastic 1 is minimally fractured, weathers spheroidally, and is seemingly unaltered beyond the effects of burial metamorphism turning volcanic glass to Fe-rich smectite, imparting the characteristic green color to the rock (Evarts and Ashley, 1993).

Two grades of contact metamorphism are present and identified as distinct lithologies. Hornfelsed (*Hornfels*) rocks have a dark grey to black, aphanitic groundmass with a shagreen texture and phenocrysts of dark brown biotite. Lower down the face of the outcrop volcaniclastic 2 (*Vcl 2*) has been turned to a darker shade of gray than the host rock (*Vcl 1*). Primary structures of the volcaniclastics are still visible, though some of the clasts are oxidized and weathered into void space. This effect is pervasive enough to warrant identification as a separate lithology, but is not so advanced as to be considered hornfels grade metamorphism.

Volcaniclastic 3 (*Vcl 3*) has a purple to purpleish-white groundmass with mineral and clastic composition apparently identical to those of *Vcl 1*. Clasts in *Vcl 3* were sometimes found to be weathering out or oxidizing, forming void spaces that are rimmed with orange staining.

The term *Boundary Alteration* is applied to discolored zones which form a boundary between Volcaniclastics 1 and 2, and also define the edges of large lobate structures. In zones of boundary alteration the primary structure of volcaniclastics is faintly visible, but the rock is bleached to a pinkish white color and are very soft, deforming as clay or putty under the point of a rock hammer. These rocks usually form a break in slope, creating relatively flat, planar surfaces surrounded by the more sheer rock faces of *Vcl 1* and *Vcl 2*.

Oxidized Volcaniclastics (*O-Vcl*) are pervasively altered to shades of yellow, white, and orange. The lithic clasts and mineral phenocrysts typical of volcaniclastics are all weathering out, and oxidation haloes around void spaces once filled by clasts are common.

The zone mapped as *Silicified Volcaniclastics* (*S-Vcl*) is a fault-bound vertical conduit which is very hard and commonly encased in quartz cement which rings when struck with a hammer.

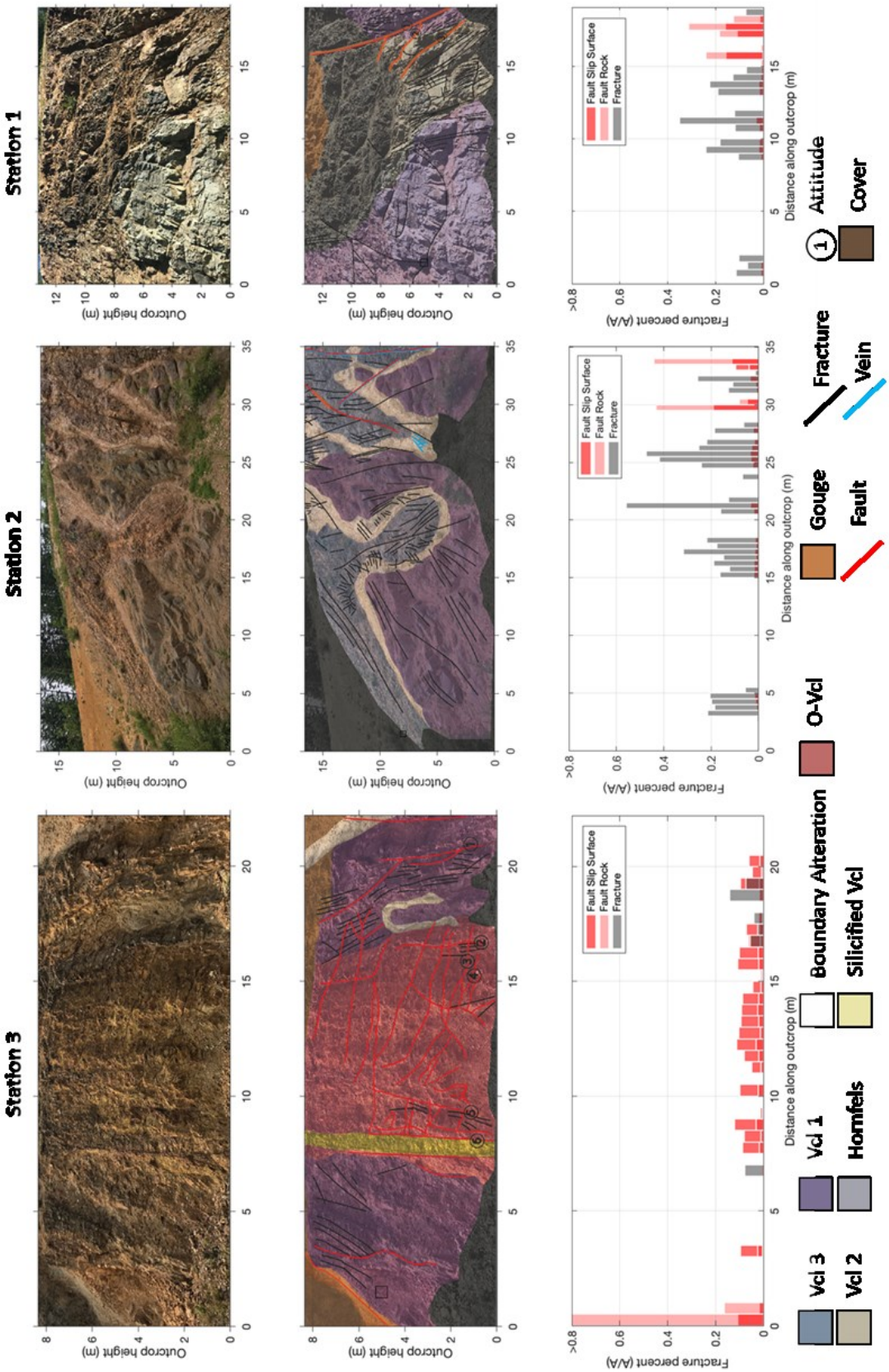

Figure 5: Outcrop 2 lithological/structural maps. Stations 1 and 2 are on the north side of Hwy. 501, and Station 3 is opposite Station 2 on the south side of the road. The histogram is calculated from a 1x1m sample window at a constant y-coordinate, with one box plotted on each map for scale and position.

3.2.6 Outcrop 2 – Structures

Station 1 is near the eastern end of the outcrop, and is dominated by a semi-circular ring of hornfels contact metamorphism from a small arm of the Spud Mt. Pluton, which outcrops above the plane of view of the outcrop maps. The hornfelsed zone is thoroughly broken by approximately perpendicular fracture sets, chopping the mapped area of this lithology into small rectangular rock masses. These features have not been individually mapped due to their ubiquitous presence and population density, which has subsequently been exacerbated by exposure to weathering, creating a new fabric altogether.

Outside of this zone, fracturing and faulting are comparatively sparse, though *Vcl 2* is marked by many sub-vertical fractures and occasional perpendicular fracture sets that may represent the incipient stages of the intense fracturing found in the hornfels.

Volcaniclastic 3 (Station 2) is cut by sets of perpendicular fracture sets into many small rectangular blocks, creating a fabric nearly identical to the intense fracturing mapped in the hornfels zone of Station 1. Zones of Boundary Alteration separate the heavily fractured and altered volcaniclastics (*Vcl 2*) and the relatively undeformed host rock (*Vcl 1*). The zones of Boundary Alteration form large, curved lobate structures which are the dominant visible feature in the outcrop. The edges of the lobate structure are defined by either: (1) veins of dark brown alteration material, likely hematite, (2) multiple planar, approximately parallel slip surfaces, or (3) a combination of 1 and 2.

Station 3 is directly across the road from the lobate structures in Station 2. The large central portion of the outcrop is pervasively altered to shades of yellow, white, and orange. These oxidized volcaniclastics (*O-Vcl*) are cut by numerous faults, identified by parallel or braided slip surfaces which are altered to a dark brown color. These faults do not have blunt tips as suggested by the outcrop map, but spread into smaller anastomosing slip surfaces branching out like roots. These features are below the resolution of the photograph but the effect is particularly visible in the eastern quadrant of the outcrop, bordering silicified volcaniclastics. These chaotic fracture networks bound the yellow/white/orange rocks on all sides. The reddish brown zones vary from <5 mm of alteration on either side of a fracture to larger than hand size. This alteration product is noticeably harder than the surrounding oxidized host rock and rings when struck with a hammer. On the eastern extent of this lithology the oxidation gradually fades away, leading into the relatively unaltered purpleish white volcaniclastics (*Vcl 1*). There is a fault-bound vertical conduit of Silicified Volcaniclastics close to the eastern edge of the Oxidized Vcl. This chimney is very hard, and in places has been almost completely remineralized to quartz.

3.2.7 Outcrop 2 – Proximity to Heat

We interpret the prominent lobate structure to be the result of alteration by an arm of the Spud Mt. Pluton further into the wall of the outcrop (Figure 6). Very near to the intrusion the country rock is metamorphosed to hornfels, or skarn. Moving further away, the heat and force of that intrusion pushing outward form these curved zones of boundary alteration, shadowed by arcuate fracture patterns in the surrounding parent material, which is intensely fragmented. As we continue to move away from the intrusion we see less of the boundary alteration and more evidence for extensive faulting and alteration from hot, acidic fluids which causes the pervasive oxidation in Station 3. The faults appear to radiate from the contact oriole providing a potential pathway for fluid migration and exchange. The locally intense alteration at their margins is also consistent with their role in hosting reactive fluid transport.

The impact of alteration on fracturing is quantitatively assessed by measuring fracture density across these alteration zones in the outcrop maps as was done form Outcrop 1 (Figure 5).

The maps and associated histograms reveal:

- Fracture density strongly correlates with alteration type: Hornfels shows the highest density typified by pervasive fracturing at the decimeter length scale, followed *Vcl 2* and *Vcl 3* with spacing at the meter length scale, and the relatively un-fractured *Vcl 1*.

- Small faults are most prominent in *O-Vcl*. In this outcrop these include the highly altered faults radiating from the intrusive body behind the plane of the outcrop.

Whereas fracture density in Outcrop 1 is highly localized near the strike slip faults in the volcanicastics, Outcrop 2 displays a dependence on alteration zones which are typified by representative fracture densities.

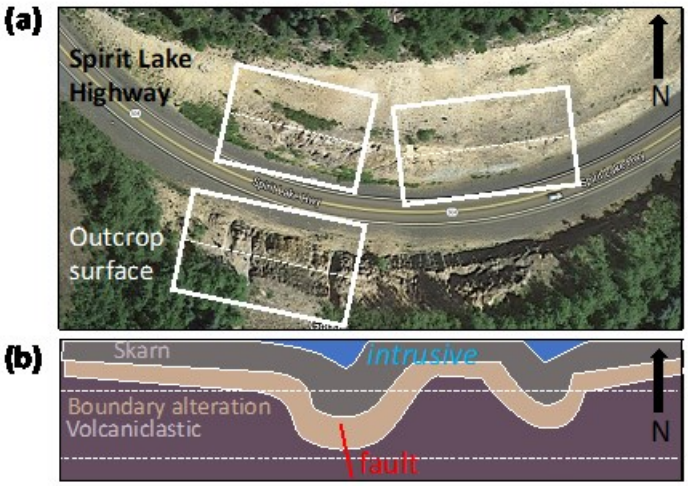

Figure 6: Map view sketch encompassing Outcrop 2, Stations 2 & 3.

3.3 Borehole Results

Data from two boreholes is being analyzed in this study. First, we examine image and geophysical property logs from PBO Borehole Strainmeter B201 to interpret the orientations of natural fractures and drilling induced structures. When planar surfaces cross-cut the borehole, they appear as sinusoids in the un-wrapped cylindrical BHTV image (e.g. Zemanek et al., 1970, Zoback, 2007 and references therein). Both natural fractures and drilling induced borehole breakouts are identified as zones of reduced acoustic amplitude, appearing darker than the adjacent borehole wall due to their increased surface roughness (Figure 7). For fractures, the trough of the sine wave represents the dip azimuth, and the dip angle is calculated as the inverse tangent of the ratio of the height of the sinusoid to the diameter of the borehole at the depth of the feature. Borehole breakouts form where the hoop stress along the borehole wall exceeds the compressive rock strength. They are recognized as regions of low amplitude with irregular edges extending along the length of the borehole (Figure 7c). Breakouts occur as pairs azimuthally aligned with the least compressive principal stress (S_{hmin}) (Gough and Bell, 1982). Thus, interpretation of these image logs reveal the orientations and apparent apertures of fractures at depth, as well as the position and attitude of lithologic boundaries (Figure 7a). The impact of these fractures on fluid flow can be assessed by comparison with the position of identified fractures with logs of sonic porosity and temperature. Second, we analyze drill cuttings and equilibrated temperature measurements from PFA site 17-24. These data sets reveal the subsurface lithology and effects of alteration, and provide a preliminary assessment for the local geothermal gradient and the likelihood of the presence of a source of heat.

3.3.1 PBO Borehole Strainmeter B201

In 2007 the Plate Boundary Observatory installed four borehole strainmeters around MSH. All four holes were drilled vertically to approximately 244 m measured depth. As part of the quality assurance procedures, all holes were surveyed with a full suite of geophysical tools and are available as open source data through UNAVCO. The logs include acoustic borehole televiewer (BHTV) and full-wave sonic (FWS) logs which reveal fracture populations and their association with lithology or petrophysical properties such as porosity. Of these four boreholes, B201 has been selected for analysis due to its proximity to PFA site 17-24 (Figure 2), and the juxtaposition in favorability between the two sites. The logged interval of B201 is from ~137 m to 244 m MD.

B201 Data Processing

For B201, one acoustic image log was downloaded and imported into WellCAD® for analysis. The log was collected using a Century Geophysical Acoustic Televiewer Logging Tool (9804), and the logged interval spans from approximately 137.5 m (depth of casing = 137.16 m) to 244 m (bottom of hole) with a maximum deviation from vertical of <2°. The borehole caliper was inferred from two-way travel time by calibration to the inner diameter (ID) of the casing captured in the image within WellCAD® to enable the calculation of natural fracture dip.

Sine waves were fit to the traces of natural fractures cross-cutting the borehole, and polygons were fit around borehole breakouts. Fractures were assigned quality rankings according to the confidence with which we believe the sine wave reflects the trace of the fracture. Factors considered in fracture ranking include contrast of the trace with the host rock, completeness of the sine wave (full trace vs. offset fracture), and goodness of fit (higher for planar features, lower for non-planar features). Breakouts were similarly assigned quality ranking depending on the certainty with which they could be identified based on morphology and occurrence in pairs separated by 180° (as per Zoback 2007 and references therein and Davatzes and Hickman, 2009). All interpreted structures were corrected from the local borehole to the global geographic reference frame using deviation from vertical and deviation azimuth relative to true North.

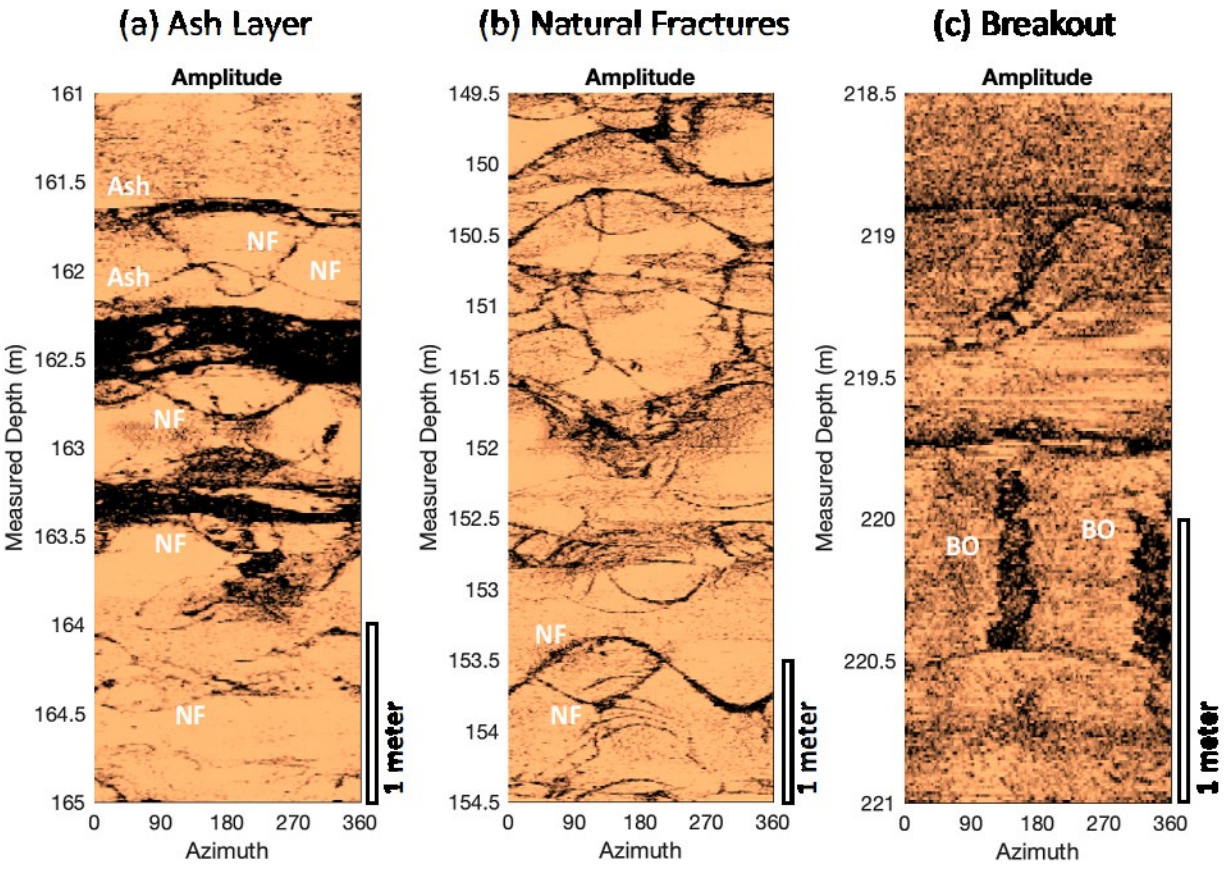

Figure 7: Example of the relationship between fractures and lithological organization. (a) Shallowly dipping ash layers (dark zone) and several abutting natural fractures within volcaniclastics (lighter image); (b) moderately dipping natural factures (darker traces) that show cross-cutting relationships in andesite. (c) Paired patches of breakouts on opposite sides of the borehole wall in andesite.

B201 Lithology

Andesite and basalt are the dominant lithologies identified by the drill log, with lesser extent of volcaniclastic and lithified ash deposits. Features separating zones of distinctly different image quality were often picked as lithologic contacts. These are usually low angle, planar features, which is consistent with outcrop observations throughout the study area (Figure 7a, Figure 8a). However, steeply dipping, non-planar surfaces have also been acknowledged as lithologic contacts based on the disparity of image quality and sonic log. Lithologies were assigned primarily by relying on the assessment of drill cuttings by the wellsite geologist. The contacts of different units were assigned according to differences in image quality, borehole diameter (from the caliper log), sonic porosity, or a combination of all three factors.

Andesites and basalts have variable image quality, with zones of low quality likely corresponding to zones of alteration, as indicated by drill log comments. Away from large fault zones, andesites and basalts are sparsely fractured (Figure 8a). Volcaniclastics and lithified ash deposits both may exhibit non-planar features which are likely cobbles and boulders. Ash layers frequently appear as washout zones where the caliper indicates borehole expansion. Many small ash beds are below the resolution which would be captured by mud logging, but are evident as thin zones where the caliper arm extends and the image log shows zones of reduced amplitude, with sub-parallel sine waves documenting the concordance of the overlying lithologic unit (Figure 7a).

B201 Natural Fractures and Drilling Induced Structures

Strike of natural fractures varies considerably over the length of the logged interval (Figure 8). The majority of the low angle features have been identified as lithologic contacts. While there is significant scatter in the remainder of the features picked as natural fractures, two populations stand out, defining conjugate sets of steeply dipping fractures which strike either NNW/SSE or ENE. Fractures often terminate at the interface between volcaniclastics and lithified ash deposits.

Two sets of breakouts have been identified in the logged interval. The shallower set are short, with low pick quality, and are aligned with an azimuth of 70°/240° at ~189 m MD. The deeper set is much more vertically extensive and represents a higher quality pick (Figure 7c). The azimuth of these breakouts is 145°/328° at 220 m MD; because of their length, the control the estimate of most compressive horizontal principal stress, S_{Hmax}, shown in Figure 8a.

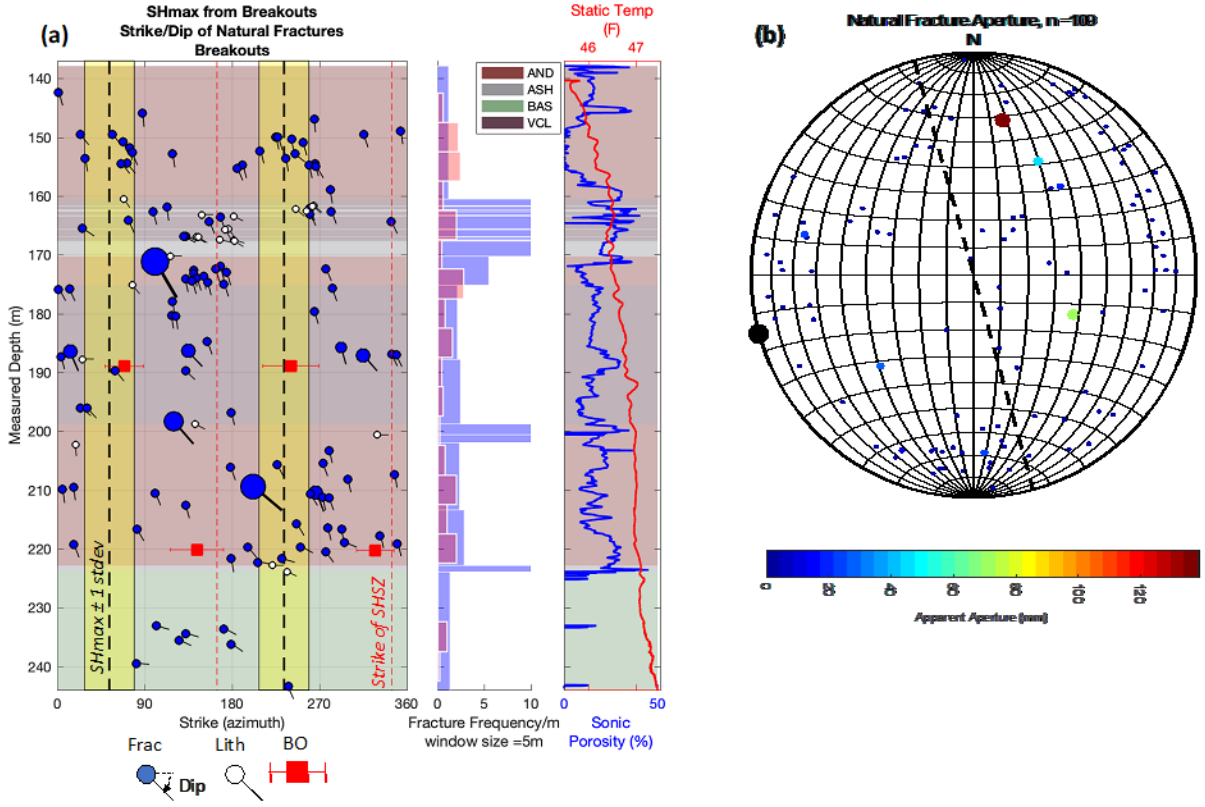

Figure 8: Summary of borehole image log interpretation. (a) Modified Tadpole plot shows the strike of natural fracture as blue dots and their dips as the tails. Dot size is proportional to apparent aperture in the image log. Stratigraphic contacts are similarly plotted in white. Breakouts are represented by red squares, and in the vertical B201 are interpreted to coincide with the minimum principal horizontal stress. The average maximum horizontal stress is then derived as the circular mean weighted by the length of breakout along the borehole ± 90°, and is 054 or 234±23.6°, although observations are sparse. The central panel denotes fracture density along the borehole, and the right panel summarizes the static temperature log along the well and sonic porosity. Background colors correspond to the prominent lithologies traversed by the well as inferred by a combination of the mud log, the image log, and the sonic and caliper logs. (b) Equal area stereogram of pole to fractures in the image log. Dot size is proportional to apparent aperture as in (a). Great circle and prominent black pole correspond to trend of the SHSZ.

3.3.2 MSH 17-24

Samples of drill cuttings were collected in real time during rotary drilling operations in the summer of 2018. These samples were assessed for mineralogy, texture, and color, then assigned a lithology based on comparison to representative local samples, and compiled into a mud log. During drilling, strong water entries lead to positive wellhead pressure below 114 meters, requiring increasing mud density with barite; this phase of drilling was also associated with significant mud loss, although the depth of the loss zones are uncertain due to the need to workover the well to manage washout. While the planned total depth (TD) for this temperature gradient hole was 488 m, site 17-24 was completed to a depth of 143 m due to repeated drilling setbacks and budget constraints. At the end of drilling, the hole was cased and cemented, and remains available for logging and possible deepening.

The depth to bedrock at site 17-24 is significantly deeper than predicted by Phase 1 and 2 exploration (Forson et al., 2017). Approximately the top 43 m is comprised of boulders and cobbles of volcaniclastics and basalt or andesite suspended in finer grained sand to clay sized sediment, all likely deposited by either the Evans Creek or the Hayden Creek glaciation events (Evarts & Ashley, 1993). Below this depth, bedrock is composed of basalt, basaltic andesite, and volcaniclastics. Basalts and basaltic andesite are comprised of plagioclase, clinopyroxenes, olivine, spinel, ilmenite, and magnetite. Volcaniclastics have mineral assemblages similar to basalts and andesites, but are distinguished based on (1) the varicolored groundmass typical of volcaniclastics, ranging from purple to green, (2) a mixture of lithologies being returned to the surface, (3) increased rate of penetration while drilling relative to basalt or andesite, and (4) the presence of XRD peaks associated with laumontite, a zeolite mineral formed by burial metamorphism of

volcaniclastic rocks of andesitic to basaltic origin (Nesse, 2000). Alteration minerals include quartz, chlorite, calcite, hematite, smectite, and illite all of which are present throughout the drilled interval.

Two temperature gradient measurements were taken in the months following the cessation of drilling at site 17-24 (Figure 19). Both show nearly isothermal temperature profiles consistent with meteoric groundwater. Given the shallow depth and artesian water entry, these results reflect the influence of local topography as well as the massive amount of meteoric water input to the area expected at these shallow depths.

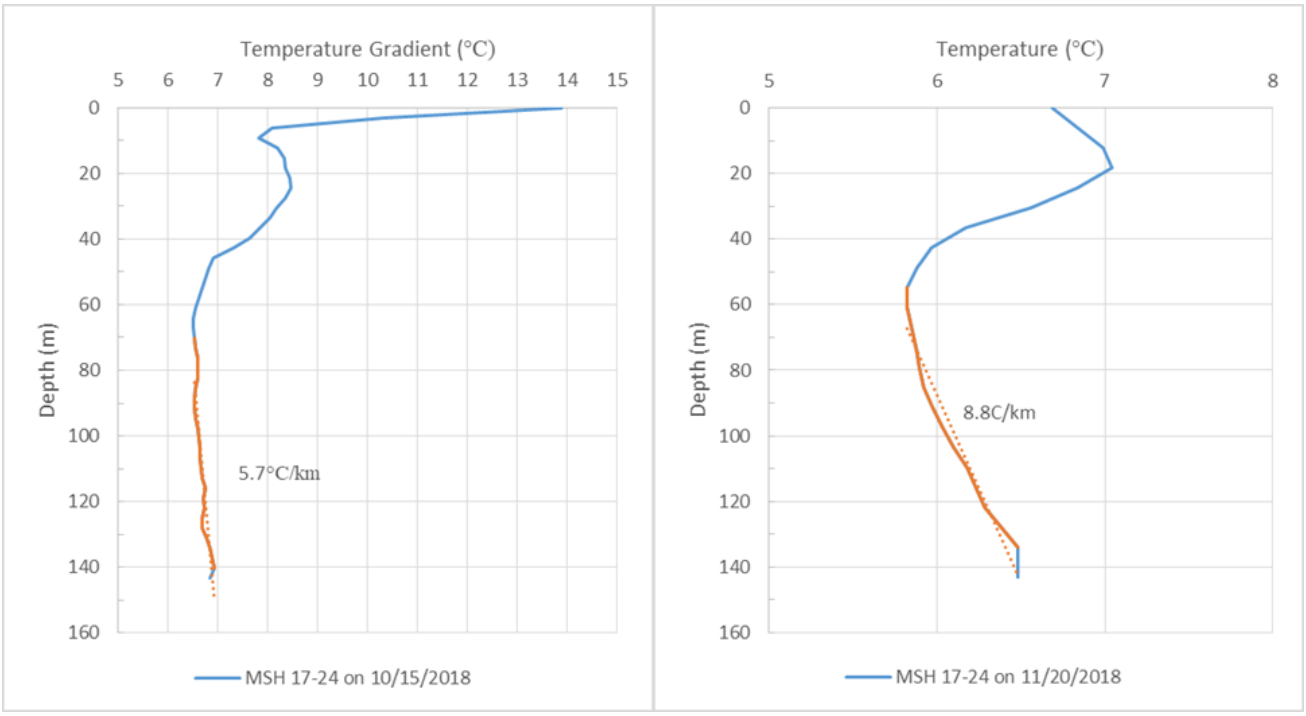

Figure 9: Temperature profiles from PFA site 17-24 taken on October 15, 2018 (left panel) and November 20, 2018 (right panel). The casing and cement in 17-24 was installed in September 2018. The later profile is considered equilibrated, which will be confirmed in late spring 2019 when the site is once again accessible.

4. DISCUSSION

From a geological perspective, geothermal reservoirs are zones where fluid is trapped and heated, and is able to be extracted to the surface (Huenges and Ledru, 2011). Defining a reservoir in terms of commerciality is more difficult, as it is dependent upon such factors as cost of extraction, size of the resource, the price of energy, etc. In order to maximize the potential for profitable energy production from the resource, a reservoir should first be in an area with a temperature gradient elevated above that of the background crustal gradient, which ranges 25-30°C/km (Fridleifsson et al., 2008). Beyond the presence of high temperature, permeability of the system is the primary limitation on the potential for geothermal energy extraction. This parameter is related to the porosity of the rock, as well as the connectivity of those pores, which is often enhanced by fractures. The upper crust has a permeability range of 10^{-17} to 10^{-14} m^2, while geothermal reservoirs are typically characterized by permeabilities of at least 10^{-13} m^2 (Brown, 1987; Barton et al., 1998; Davatzes et al., 2010; Davatzes and Hickman, 2010; Huenges and Ledru, 2011). Because drilling and completion costs routinely account for approximately 50% of the total capital investment necessary to start a geothermal power plant (Blankenship et al., 2005; Lukawski et al., 2014) the hot, porous, and permeable reservoir should then be at depths which are accessible by drilling; 2-3 km is a typical production depth for geothermal reservoirs (Fridleifsson and Freeston, 1994). For production of electricity, geothermal gradients in excess of 50°C/km are desired in order to sufficiently heat reservoirs at these depths (Huenges and Ledru, 2011). Finally, the fractures which often maintain reservoir scale permeability should be in an orientation which is likely to be critically stressed under the modern stress field, in order to ensure those pathways remain open and free of secondary mineral healing (Huenges and Ledru, 2011).

In the analyses presented here, we (1) constrain the architecture of potential reservoirs, (2) detail the fracture paragenesis as it relates to the generation of connected porosity, (3) provide new constraints on the regional geomechanical model, and (4) present preliminary findings on the likelihood of the presence of a source of heat.

4.1 Is a fractured reservoir viable in the SHSZ?

Commercial geothermal systems are found where heat is connected to a shallow, porous, and saturated reservoir via a permeable pathway (Huenges and Ledru, 2011). At Mount St. Helens, the conceptual model for geothermal systems is that heat is derived from young dikes and sills related to the magmatic plumbing system at depths greater than practical for drilling (Forson, 2015). The SHSZ provides vertically extensive conduits along which meteoric water may migrate to depth and be warmed by the intrusives then rise to

shallow depths. Candidates for reservoir rock include marine meta-sediments extrusive flows, indurated volcaniclastic deposits and lithified ash beds. These reservoir rocks should be overlain by a clay-rich, hydrothermally altered caprock. This study addresses the potential role of extrusive volcanics as a fractured reservoir rock or in allowing vertical circulation of hot fluid, taking advantage of their exposure at the surface. However, due to their greater depth and thus potential for heating the underlying meta-sediments remain a critical reservoir target.

Repeated slip along faults in the SHSZ maintains connected porosity in these initially low permeability lithologies (Forson, 2015; Forson et al., 2015; Forson et al., 2016; Forson et al., 2017; Swyer, et al., 2016) by reactivating fractures which are critically oriented for failure (i.e. Barton et al., 1995) (Figure 1), resulting in a shallow resource supplied by heat from depth.

Our field investigations and borehole analysis show that that the lithologic units and depositional environment typical in the SHSZ define a mechanical stratigraphy that is likely to control reservoir structure. Repeated sequences volcaniclastics draped by ashfall overlain by basalt or andesite flows are common throughout the field area representing significant stratigraphic thickness, as well as at depth in wells B201 and 17-24 (Evarts et al., 1987; this study). Basalt and andesite flows sometimes form columnar joints through cooling and contraction, but in many outcrops such joint are only poorly developed or absent. Otherwise, extrusive flows are sparsely fractured except by the large strike slip faults (Figure 3, Stations 3 and 4), less common locally developed minor normal faults (Figure 3, Stations 1 and 2), and the effects of exposure and weathering. Although individual flows are 2-6 m thick, accumulated sequences of basalt or andesite flows with intervening ash and volcaniclastics exceed 300 m in thickness (Evarts & Ashley, 1993). Locally, flow thickness is likely to have been controlled by paleo-topography (e.g., Figure 3). Volcaniclastics in the SHSZ vary widely in their description, but the most commonly encountered types are similar to the welded tuffs described in Outcrop 1. These units typically display well-developed, distributed fractures, as well as localized damage adjacent to strike slip faults and a complex paragenesis consistent with persistent fracture dilation. They are consistently more densely fractured than basalts or andesites (Figure 3, bottom row; Figure 8a). Lithified ash deposits clearly drape paleo-topography in layers a few meters or less thick. While fractures and faults do occasionally cut into and through ash layers, strain is more often accommodated by this weak layer slipping preferentially along depositional planes, rather than undergoing brittle fracture (Figure 3, Stations 1 and 2; Figure 8a).

All of these lithologies have very low primary porosity (e.g., Figure 4), but there is ample evidence for porosity due to dilation of fractures. These fractures show evidence for multiple generations of slip and healing suggesting that fractures act as preferred and persistent conduits for fluid flow. Quartz cement is consistent with precipitation from cooling fluid such as water migrating upward from depth, dolomite from hydrothermal alteration, and iron oxide (hematite) from oxygenated meteoric waters. All this is indicative of natural fractures acting as preferred pathways for fluid flow over an extended period of time and distance (e.g. Eichubl et al., 2009).

Thus, these three distinct lithologic units in their repeated sequence define a mechanical stratigraphy controlling fracture porosity and connectivity. While potential reservoirs are likely to be compartmentalized by common lithologic packages of extrusive flows, indurated volcaniclastics, and lithified ash layers defining the potential reservoir storage, steeply dipping strike-slip faults that cut this stratigraphy provide the means to bypass this compartmentalization and facilitate migration of hot fluid to shallow depth. Borehole image logs necessarily under-sample steeply dipping features near the borehole, so we can assume that this effect is more pronounced than our analysis indicates. Locally, alteration around these fractures is consistent with their role in facilitating vertical fluid exchange. For both the strike slip faults and distributed fractures, repeated cementation documents cycles of porosity rejuvenation due to fracture reactivation.

Outcrop 2 (Figure 5) reveals that high fracture density is associated with the margin of intrusive bodies in volcaniclastics and adjacent contact metamorphism. Alteration and cementation in and adjacent to these fractures indicate that they played a key role in hosting fluid circulation and heat exchange as proposed by the PFA model. Together the mechanical stratigraphy explored in Outcrop 1 and persistent permeability of fractures adjacent to the intrusive heat source in Outcrop 2 provide key ingredients to support geothermal systems in the SHSZ.

Although the seismicity in the SHSZ documents active slip on strike-slip faults (Figure 2), it does not reveal whether those faults dilate and host fluid flow. Alteration associated with fractures in outcrop reveal their role in hosting paleo-fluid flow, but not whether they are active today. The depths accessed by B201 provide an opportunity to test whether fractures in this region are in an orientation favorable for reactivation based on either the local measurement of S_{Hmax} azimuth inferred from breakout or that modeled by the PFA and others from plate convergence or geodetic strain rate measured on the regional Plate Boundary Observatory GPS array (e.g., Swyer et al., 2016). Borehole breakout indicates S_{Hmax} azimuth of 054/234°±23.6°. This azimuth is consistent with a stress state governed by the influence of plate subduction, where the azimuth of S_{Hmax} is 055° (Evarts and Ashley, 1987 and references therein). This differs slightly from stress models explored by Swyer et al. (2016), which infer 028° from instantaneous strain from raw GPS velocities. In both cases, many natural fractures in B201 (including several of the prominent large apparent aperture fractures) and strike slip faults in Outcrop 1 are well-oriented for strike slip, suggesting they may continue to be active today. The conjugate sets of steeply dipping fractures which define a significant portion of the population (Figure 8) are, most consistent with the compressive horizontal stress 028° modeled by the PFA (Swyer et al., 2016), whereas only one set is reasonably well-oriented for an azimuth of 054°.

4.1 Is there heat accessible in the SHSZ?

At the depths to which our investigations extend there is not an elevated temperature gradient reflecting close proximity to a source of heat. However, that is to be expected at these shallow depths given the abundance of cold, meteoric water input from precipitation in the Cascades and encountered during drilling. Although heat has yet to be found, this result does prove fluid saturation of the subsurface fracture population and host rocks. There is similarly as yet no evidence for a hydrothermally altered, clay-rich caprock at these depths

consistent with the presence of geothermal system in the past at the site of B201 or 17-24. Trace amounts of zeolites, illite, and smectite are present sporadically throughout the drill cuttings, but these are more likely derived from burial metamorphism or weathering at the surface.

5. CONCLUSION

The extrusive volcanic sequences in the SHSZ north of MSH comprise a mechanical stratigraphy which is likely to control reservoir compartmentalization. Networks of connected fractures constitute potential reservoir storage and are oriented well to be reactivated and dilate in today's stress state, as established by our new borehole observations and by geodetic studies. This is consistent with the high rate of seismicity throughout the SHSZ. In addition, localized alteration documents the past role of these fractures in hosting fluid flow. Together, these fracture characteristics and current seismic activity are likely to promote circulation of hot fluids from greater depths into a shallow reservoir zone. Saturation of the system appears ensured by the massive amount of precipitation which the region sustains, and is evidenced in the subsurface by artesian fluid flow in groundwater aquifers encountered during drilling. As yet, our investigations have not reached below the influence of these shallow aquifers to assess the presence of heat, though this remains a primary goal of the continuation of Phase 3 exploration of the PFA.

6. ACKNOWLEDGEMENTS

This work was supported by a grant from the Department of Energy's Geothermal Technologies Office. Access to field sites was provided by Weyerhauser Corporation and Noble Farms. Furthermore, the study would not have been possible without involvement of the Washington Geological Survey, AltaRock Energy, the USGS Western Research Drilling Program. Peter Stelling, Nikhil Amin, and Molly Johnson from Western Washington University, and Matt Uddenberg of Stravan Consulting, LLC all provided invaluable field support during Phase 3 exploration.

REFERENCES

Anderson, Kyle, and Paul Segall. "Bayesian inversion of data from effusive volcanic eruptions using physics-based models: Application to Mount St. Helens 2004–2008." *Journal of Geophysical Research: Solid Earth* 118, no. 5 (2013): 2017-2037.

Barker, Sally E., and Stephen D. Malone. "Magmatic system geometry at Mount St. Helens modeled from the stress field associated with posteruptive earthquakes." *Journal of Geophysical Research: Solid Earth* 96, no. B7 (1991): 11883-11894.

Barton, Colleen A., Mark D. Zoback, and Daniel Moos. "Fluid flow along potentially active faults in crystalline rock." *Geology*23, no. 8 (1995): 683-686.

Barton, Colleen A., S. H. Hickman, Roger Morin, Mark D. Zoback, and Dick Benoit. "Reservoir-scale fracture permeability in the Dixie Valley, Nevada, geothermal field." In *SPE/ISRM Rock Mechanics in Petroleum Engineering*. Society of Petroleum Engineers, (1998).

Batir, Joseph, Nicholas C. Davatzes, and Ragnar Asmundsson. "Preliminary model of fracture and stress state in the Hellisheidi Geothermal Field, Hengill Volcanic System, Iceland." In *Proceedings of the Thirty-Seventh Workshop on Geothermal Reservoir Engineering, Stanford*. 2012.

Blankenship, D. A., J. L. Wise, S. J. Bauer, A. J. Mansure, R. A. Normann, D. W. Raymond, and R. J. LaSala. "Research efforts to reduce the cost of well development for geothermal power generation." In *Alaska Rocks 2005, The 40th US Symposium on Rock Mechanics (USRMS)*. American Rock Mechanics Association, 2005.

Brown, Stephen R. "Fluid flow through rock joints: the effect of surface roughness." *Journal of Geophysical Research: Solid Earth* 92, no. B2 (1987): 1337-1347.

Davatzes, N. C., M. Swyer, D. A. Lockner, J. G. Solum, and N. Anyamele. "Mechanisms of fault gouge evolution and physical properties." In *AGU Fall Meeting Abstracts*. 2010.

Davatzes, N. C., & Hickman, S. (2010). The feedback between stress, faulting, and fluid flow: Lessons from the Coso Geothermal Field, CA, USA. In *Proceedings World Geothermal Congress 2010* (pp. 1-14).

Eichhubl, Peter, Nicholas C. Davatz, and Stephen P. Becker. "Structural and diagenetic control of fluid migration and cementation along the Moab fault, Utah." *AAPG bulletin* 93, no. 5 (2009): 653-681.

Evarts, Russell C., Roger P. Ashley, and James G. Smith. "Geology of the Mount St. Helens area: Record of discontinuous volcanic and plutonic activity in the Cascade Arc of southern Washington." *Journal of Geophysical Research: Solid Earth* 92, no. B10 (1987): 10155-10169.

Evarts, Russell C., and Roger Parkmand Ashley. *Geologic map of the Spirit Lake West quadrangle, Skamania and Cowlitz Counties, Washington*. The Survey, 1993.

Forson, C.. Phase 1 Technical Report. *Unpublished*. Washington Division of Geology and Earth Resources. (2015) DE-EE0006728. FY2015, Q3.

Forson, C., J. L. Czajkowski, D. K. Norman, M. W. Swyer, T. T. Cladouhos, and N. Davatzes. "Summary of Phase 1 and Plans for Phase 2 of the Washington State Geothermal Play-Fairway Analysis." *Geothermal Resources Council Transactions* 40 (2016): 541-550.

Forson, C., Steely, A.N., Cladouhos, T., Swyer, M., Davatzes, N., Anderson, M., Ritzinger, B., … & Stelling, P.. Geothermal Play-Fairway Analysis of Washington State Prospects: Phase 2 Report and Phase 3 Proposal. *Unpublished,* (2017)1-52.

Forson, C., Swyer, M. W., Schmalzle, G. M., Czajkowski, J. L., Cladouhos, T. T., Davatzes, N., ... & Cole, R. A.. Geothermal Play-Fairway Analysis of Washington State Prospects. *Geothermal Resources Council Transactions*, *39* (2015), 701-710.

Fridleifsson, Ingvar B., and Derek H. Freeston. "Geothermal energy research and development." *Geothermics* 23, no. 2 (1994): 175-214.

Fridleifsson, Ingvar B., Ruggero Bertani, Ernst Huenges, John W. Lund, Arni Ragnarsson, and Ladislaus Rybach. "The possible role and contribution of geothermal energy to the mitigation of climate change." In *IPCC scoping meeting on renewable energy sources, proceedings, Luebeck, Germany*, vol. 20, no. 25, pp. 59-80. Citeseer, 2008.

Gough, D. I., and J. S. Bell. "Stress orientations from borehole wall fractures with examples from Colorado, east Texas, and northern Canada." *Canadian Journal of Earth Sciences* 19, no. 7 (1982): 1358-1370.

Huenges, Ernst, and Patrick Ledru, eds. *Geothermal energy systems: exploration, development, and utilization*. John Wiley & Sons, 2011.

King, Geoffrey CP, Ross S. Stein, and Jian Lin. "Static stress changes and the triggering of earthquakes." *Bulletin of the Seismological Society of America* 84, no. 3 (1994): 935-953.

Laubach, Stephen E., Jon E. Olson, and Michael R. Gross. "Mechanical and fracture stratigraphy." *AAPG bulletin* 93, no. 11 (2009): 1413-1426.

Lukawski, Maciej Z., Brian J. Anderson, Chad Augustine, Louis E. Capuano Jr, Koenraad F. Beckers, Bill Livesay, and Jefferson W. Tester. "Cost analysis of oil, gas, and geothermal well drilling." *Journal of Petroleum Science and Engineering*118 (2014): 1-14.

McGarr, Arthur, and N. C. Gay. "State of stress in the Earth's crust." *Annual Review of Earth and Planetary Sciences* 6, no. 1 (1978): 405-436.

Moos, D., R. D. Jarrard, T. S. Paulsen, E. Scholz, and T. Wilson. "Acoustic borehole televiewer results from CRP-2/2A, Victoria Land Basin, Antarctica." *Terra Antartica* 7, no. 3 (2000): 279-286.

Swyer, M. W., T. T. Cladouhos, C. Forson, J. L. Czajkowski, N. C. Davatzes, and G. M. Schmalzle. "Permeability potential modeling of geothermal prospects combining regional crustal strain rates with geomechanical simulation of fault slip and volcanic center deformation: A case study for Washington State geothermal play fairways." In *50th US Rock Mechanics/Geomechanics Symposium*. American Rock Mechanics Association, 2016.

Swyer, Michael W., Matthew E. Uddenberg, Trenton T. Cladouhos, Alexander N. Steely, Corina Forson, and Nicholas C. Davatzes. "Preliminary Geothermal Resource Assessment of the St. Helens Seismic Zone Using the Results from the Geothermal Play-Fairway Analysis of Washington State Prospects." In *PROCEEDINGS, 44th Workshop on Geothermal Reservoir Engineering Stanford University, Stanford, California, February 12-14*. 2018.

Tembe, Sheryl, David A. Lockner, and Teng-Fong Wong. "Effect of clay content and mineralogy on frictional sliding behavior of simulated gouges: Binary and ternary mixtures of quartz, illite, and montmorillonite." *Journal of Geophysical Research: Solid Earth* 115, no. B3 (2010).

Waite, Gregory P., and Seth C. Moran. "VP Structure of Mount St. Helens, Washington, USA, imaged with local earthquake tomography." *Journal of Volcanology and Geothermal Research* 182, no. 1-2 (2009): 113-122.

Weaver, Craig S., and Stewart W. Smith. "Regional tectonic and earthquake hazard implications of a crustal fault zone in southwestern Washington." *Journal of Geophysical Research: Solid Earth* 88, no. B12 (1983): 10371-10383.

Weaver, C. S., Grant, W. C., & Shemeta, J. E. (1987). Local crustal extension at Mount St. Helens, Washington. *Journal of Geophysical Research: Solid Earth*, *92*(B10), 10170-10178.

Wells, O.L., Davatzes, N.C.. The History of Dilation Across Natural Fractures Due to Evolving Surface Roughness. *Proceedings, Fourtieth Workshop on Geothermal Reservoir Engineering*. Stanford University. (2015)

Zemanek, Joe, E. E. Glenn, L. J. Norton, and R. L. Caldwell. "Formation evaluation by inspection with the borehole televiewer." *Geophysics* 35, no. 2 (1970): 254-269.

Zhu, T.Y., , Some useful numbers on the engineering properties of Materials (geologic and otherwise), GEOL 615, Department of Geophysics, Stanford University.(2012)

Zoback, Mark D. *Reservoir geomechanics*. Cambridge University Press, 2010.